공학석사 학위논문

Heating characteristics of $Fe@Fe_3O_4$ core shell nanoparticles under NIR laser irradiation or external AC magnetic field applying

근적외선 (NIR) 레이저 조사 또는 외부 AC 자기장 적용 하에서 $Fe@Fe_3O_4$ 코어 껍질 나노 입자의 가열 특성

2019 년 2 월

서울대학교 융합과학기술대학원

융합과학부 나노융합전공

구 창 혁

Heating characteristics of $Fe@Fe_3O_4$ core shell nanoparticles under NIR laser irradiation or external AC magnetic field applying

지도 교수 박 원 철

이 논문을 공학석사 학위논문으로 제출함
2018 년 12 월

서울대학교 융합과학기술대학원
융합과학부 나노융합전공
구 창 혁

구창혁의 공학석사 학위논문을 인준함
2018 년 12 월

위 원 장 김 연 상 (인)

부위원장 박 원 철 (인)

위 원 이 강 원 (인)

Abstract

Heating characteristics of $Fe@Fe_3O_4$ core shell nanoparticles under NIR laser irradiation or external AC magnetic field applying

Changhyuk KOO
Program in Nano Science and Technology
Graduate School of Convergence Science & Technology
Seoul National University

Among the number of hyperthermia materials, magnetic nanoparticles have received much attention. In this work, we studied the heating characteristics of $Fe@Fe_3O_4$ core-shell nanoparticle under near infrared laser irradiation and external AC magnetic field applying.

$Fe@Fe_3O_4$ core-shell nanoparticles were prepared by thermal decomposition of iron pentacarbonyl and followed by controlled oxidation. The prepared uniform particles were further coated with dimercaptosuccinic acid to make them well dispersed in water. Near infrared derived photothermal study of solutions containing different concentration of the core shell nanoparticles was made by using 808 nm laser source. Additionally, magnetic hyperthermia ability of the $Fe@Fe_3O_4$ nanoparticle at 150 kHz and various oersted (140 ~ 180 Oe) condition was systemically characterized. The $Fe@Fe_3O_4$ nanoparticles which exhibited effective photo and magnetic hyperthermia is expected to be used in bio medical application..

Keywords: Magnetic material, core shell nanoparticle, surface modification, Magnetic hyperthermia, Photothermal hyperthermia.

Student Number: 2017-25795

Contents

List of Figures

List of Tables

Chapter 1. Introduction

Nanoparticles, such as silica, iron oxide, zinc oxide and gold nanoparticles, have attracted much research interest for various bio medical applications, for instance, bio imaging1−4, hyperthermia treatment5−8 and other therapeutic applications.9−12 Especially, many kinds of photo and magnetic hyperthermia nanomaterials have been investigated these days. Near infrared laser and external magnetic field which are normally used in this application are known as less harmful to human body and possess effective cancer cell killing ability.

Regarding to hyperthermia treatment, gold nanoparticles are known as the most effective photothermal material due to the surface plasmon phenomenon which enhancing the photothermal effect. However, the mechanical weakness of gold nanoparticles limited their actual applications in biomedical field. Therefore, many efforts have been made to prepare new photothermal materials with enhanced mechanical strength.13−16

Unlike gold nanoparticles which possess mechanical weakness in photothermal process, most of the magnetic nanoparticles do not shows obvious morphology changed during magnetic hyperthermia

experiments. In recently years, many researches have been made to prepare magnetic nanoparticles with high magnetic saturation value17,18 for more effective heat generation19-21.

Among the various materials that meet above purpose, iron nanoparticles are characterized by their inherent strong magnetism and material rigidity. However, iron itself is easily oxidized under air or water exposure condition. As a result, many research works have been made to improve the stability of iron nanoparticles. According to improve the stability of iron nanoparticles, the nanoparticles further coated with other material and carbon, silica or other metal oxide are routinely used as candidate materials.22–25

In this work, we studied the heating characteristics of uniform Fe@Fe_3O_4 core-shell nanoparticle under near infrared laser irradiation and external AC magnetic field applying. Fe@Fe_3O_4 core shell nanoparticles were prepared by thermal decomposition of iron pentacarbonyl and controlled oxidation of iron edge.26,27 According to the TEM images, the synthesized nanoparticle size was measured with total size of 14.9 ± 1.2 nm with core size 9.6 ± 1.1 nm. Vibrating-sample magnetometer shows that magnetic saturation value of the pristine Fe@Fe_3O_4 nanoparticles was measured as 83.3 emu/g.

The $Fe@Fe_3O_4$ nanoparticles were further coated with dimercaptosuccinic acid (DMSA) to obtain water dispersity. Photothermal ability study of the coated nanoparticle was conducted at various laser power and concentration. To understand the heating ability of the synthesized nanoparticle via quantitative analysis, heat conversion efficiency was calculated by simple mathematical method and the calculated efficiency were measured at a maximum of 33.21% and a minimum of 20.79% under various experimental conditions. Moreover, the magnetic hyperthermia test was operated at 150 kHz with various oersted (140-180 Oe) condition. The particles show perfect cycle stability during 5 times repeating photothermal test.

Chapter 2. Experiment

2.1 Materials

Iron pentacarbonyl (Fe(CO)5), Oleylamine (OAm, purity 70%), 1-octadecne (ODE, purity 90%) , DMSA and hexadecylamine (HDA, purity 95%) were purchased from Sigma−Aldrich. Trimethylamine N-oxide (purity 95%) were obtained from TCI. Dimethyl sulfoxide (DMSO, purity 90%) were obtained from JUNSEI.

\

2.2 Characterization

Transmission electron microscopy (TEM) images were carried out by a LIBRA 120 Energy-filtering transmission electron microscope at an acceleration voltage of 120kV. X-ray diffraction pattern were measured by Buker New D8 Advance model using Cu Kα radiation (λ = 0.15418 nm). Hysteresis loop were obtained from vibrating sample magnetometer (VSM) by Lake shore VSM − 7410. The hydrodynamic size distribution and zeta potential data of the Fe@Fe_3O_4 measured by dynamic light scattering using a Zetasizer Nano ZS. UV spectrum were investigated by PerkinElmer Lambda 35 UV / VIS spectrometer. The photothermal test were studied by PSU-W-FC laser power supply. The AC magnetic induced heating characteristics of nanoparticles were measured by using specially designed HF induction generator. HF induction generator consists of AC coils, DC power supplies, water chiller, capacitor, optical thermometers, function generators, and a PC system. This device operates 30-150 kHz of frequencies and 80-200 Oe of magnetic field strength.

2.3 Synthetic route for $Fe@Fe_3O_4$ nanoparticles

Make a mixed solution of 1-octadecene(20mL) and oleylamine (0.3mL) in a three neck flask, 280mg of HDA · HCL (HDA · HCL were prepared by followed previous research work by Lacroix26 was added to the above solution. The solution was heated to 120℃ under nitrogen atmosphere. Maintaining the temperature for 30min to degas the solution. After that, the temperature of the mixture increased to 180℃ when the temperature reached to 180℃, adding 0.7mL of Fe(CO)5 and reacted 30min. After 30min, reaction solution was cooled down to 100℃ and adding 7.5mg of Trimethylamine N-Oxide. And heated up to 250℃ and keep this temperature for 30min.

2.4 Surface modification of synthesized nanoparticle

The synthesized Fe@Fe_3O_4 particles were washed with ethanol for 3 times and redispersed in 5ml of toluene. The, 50mg of DMSA and 5ml of dimehtyl sulfoxide (DMSO) were added to the solution and further stirring for 48hours.

2.5 Laser irradiation and photothermal effect study

To measure the heating characteristics of the $Fe@Fe_3O_4$ core-shell nanoparticles under NIR laser irradiation, 1ml of $Fe@Fe_3O_4$ core/shell nanoparticle dispersion was added in an optical cuvette and irradiated by a NIR laser at 808 nm. The temperature of the solution was measured by a thermometer for every 30 seconds. The laser power and the concentration of the solution were tuned during the test to study the relationship of these factors.

2.6 Magnetic hyperthermia effect study under applied AC magnetic field

The heating characteristics of the $Fe@Fe_3O_4$ core shell nanoparticles were measured by AC magnetic field. In the middle of the coil, 1 mL of the nanoparticle dispersion was detected by a thermo optical sensor. The temperature of the solution was measured under magnetic field strength at 140, 150, 160, 170, and 180 Oe with fixed frequency at 150 kHz. The total measured time was 1000 seconds. We used 600 sec for heating the solution, and 400 sec for cooling the solution.

Chapter 3. Results and Discussion

3.1 Synthesis and characterization of $Fe@Fe_3O_4$ particles

We followed previously reported article.26 Schematic procedure for preparing nanoparticle and their hyperthermia application are depicted in Figure 1. The $Fe@Fe_3O_4$ core shell nanoparticles were prepared by thermal decomposition of iron pentacarbonyl and controlled oxidation of iron edge. Iron pentacarbonyls in the presence of 1-octadecene, oleylamine and hexadecyl ammonium choloride at 180 ℃ under nitrogen atmospheric condition, it thermally decomposed and composite pure body centered cubic iron nanoparticle. After the reaction, synthesized iron nanopaticles were further reacted with trimethylamine N-oxide at 250 ℃ for 30 minute for improving stability via making iron oxide shell from partial oxidation of iron edge.

To characterize the synthesized nanoparticle, we used several analytical methods such as TEM, VSM and XRD. TEM was used to figure out the size and morphology of the synthesized nanoparticles. The TEM images of the synthesized $Fe@Fe_3O_4$ nanoparticles and their size histogram obtained from the image were shown in Figure 2.

Because of the different electric conductivity between iron core and iron oxide shell, we can observe certain contrast difference within the nanoparticle by TEM images. XRD pattern of the Fe@Fe_3O_4 nanoparticle is shown in Figure 3c. The experimental result shows that major peaks of the nanoparticle are well matched with the body centered cubic Fe (PDF 00-006-0696) and Fe3O4 nanoparticle (PDF 00-065-0731). This XRD analysis data also supports the fact that the synthesized nanoparticles contains both iron and iron oxide phase. According to Figure 2, the average diameter of nanoparticles calculated from TEM image was measured to be 14.9 $\pm$ 1.2 nm with core size of 9.6 $\pm$ 1.1. Although the difference between the total and the core size of the synthesized nanoparticles varies great, the standard deviation difference is not significant. This is because the oxidation reaction of core iron were hindered due to the formation of iron oxide shell which prohibited penetration of oxidant into inner iron core layer. Therefore, after the formation of the certain thickness of the shell, oxidation reaction will not occur anymore and so that the nanoparticles have similar shell thickness. as the results of this phenomenon, the standard deviations of total size and core size is similar value. For further understanding about Fe@Fe_3O_4

nanoparticles, magnetic properties were characterized using vibrating sample magnetometer (VSM). The results obtained from VSM analysis is shown in Figure 3-a and also the Figure contains the images which also shows the response of $Fe@Fe_3O_4$ what dispersed in water by external permanent magnet. The magnetic saturation of $Fe@Fe_3O_4$ nanoparticles was 83.3 emu/g and this value is similar to that of bulk iron oxide particles.

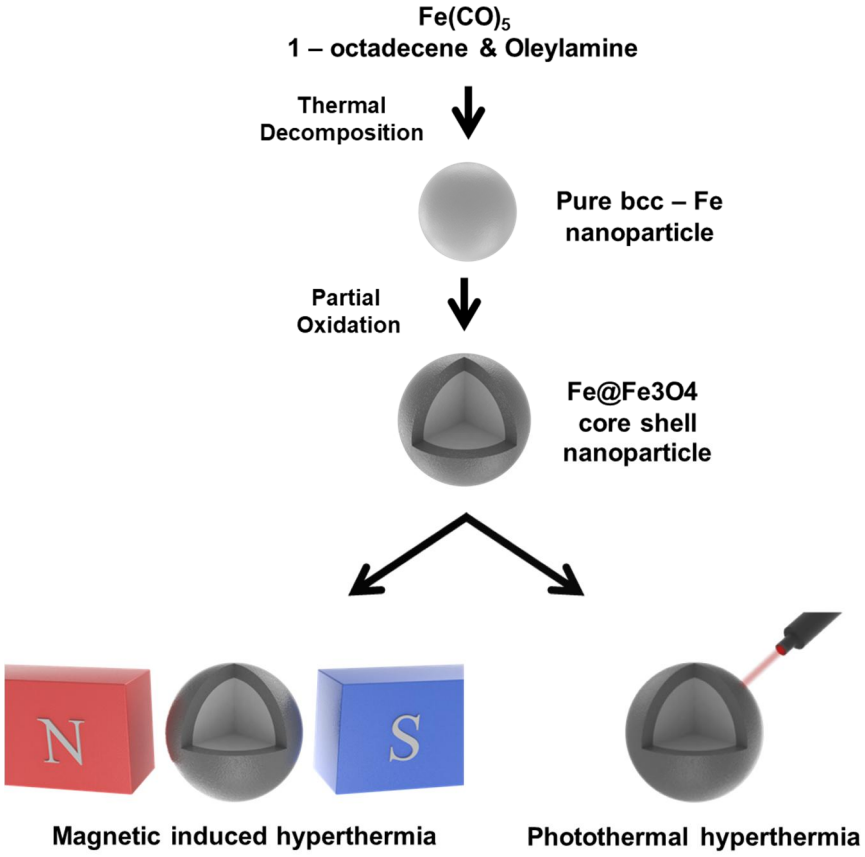

Figure 1 Schematic illustration for the synthesis of $Fe@Fe_3O_4$ core-shell nanoparticle and their hyperthermia application.

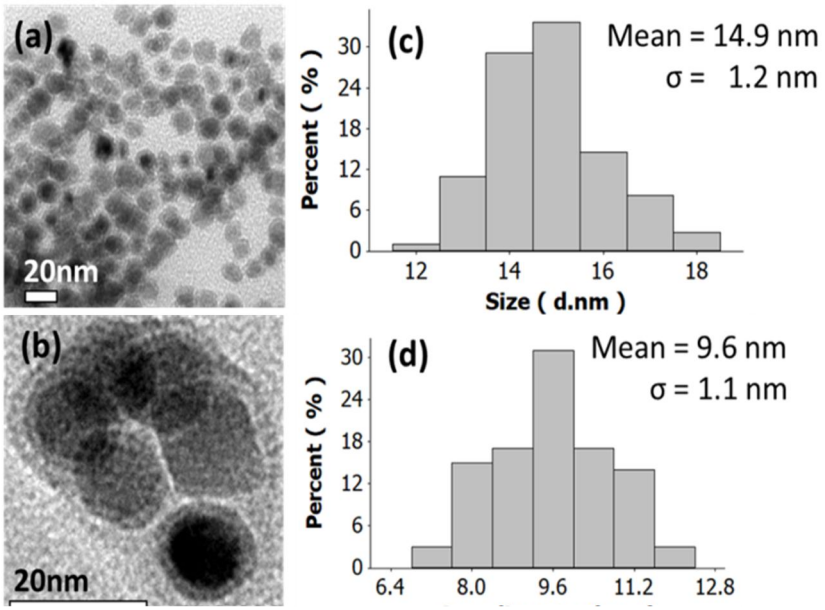

Figure 2 (a) Low and (b) relatively high magnification TEM images of the synthesized Fe@Fe_3O_4 nanoparticles prepared via thermal decomposition of iron pentacarbonyl. Size histogram of (c) whole particles and (d) the iron core.

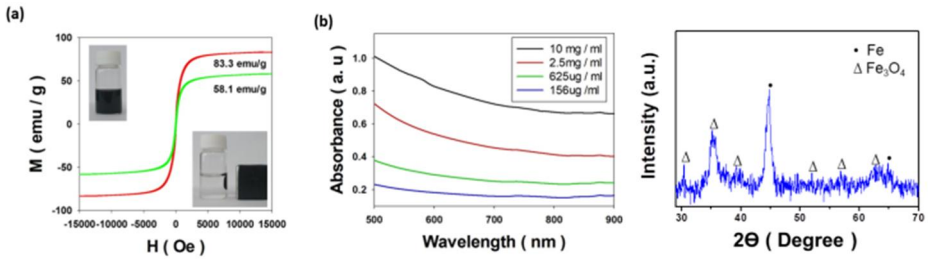

Figure 3 Hysteresis curve of (a) the synthesized Fe@Fe_3O_4 nanoparticles and the particles after coated with DMSA (insert shows the nanoparticle dispersion response to outer permanent magnet). (b) Plots of absorbance spectrum according to the concentration of the DMSA coated particle dispersion, and (c) XRD pattern of the Fe@Fe_3O_4 nanoparticle.

3.2 DMSA coating process for water dispersion

Dimercaptosuccinic acid(DMSA) coating process are commonly used to give water dispersivity to the nanoparticles.28−30 Therefore, the Fe@Fe_3O_4 nanoparticle were coated with DMSA to ensure the particle to be well dispersed in water for further experiments. The colloidal stability of the surface coated Fe@Fe_3O_4 nanopartcles were investigated by DLS and zeta potential measurements via Zetasizer Nano ZS. DLS measurements and zeta potential data are shown in Figure 4, and the DLS data of the DMSA coated Fe@Fe_3O_4 nanoparticles which shows narrow hydrodynamic size distribution is indicate that the nanoparticles are well dispersed in distilled water. Moreover, the coated nanoparticles have negative zeta potential value (-23.5 mV) due to their carboxylate end. Even though the DMSA attached particles has lower saturation magnetization than that of pristine nanoparticle, the saturation magnetization value of coated nanoparticles is steel higher compared to than that of iron oxide nanoparticles which has similar diameter.

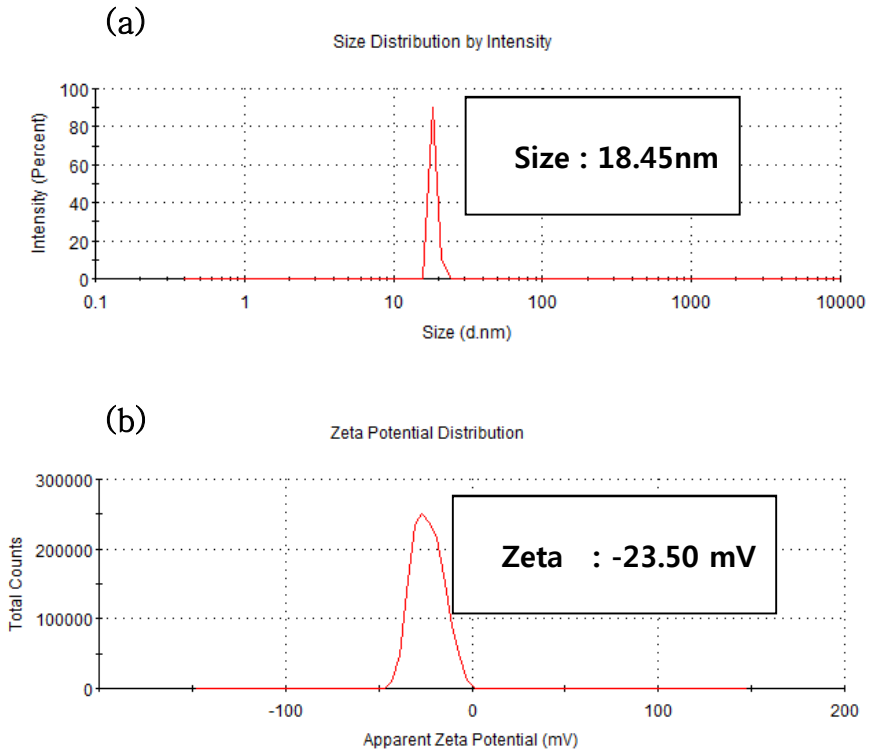

Figure 4. Dynamic light scttering(DLS) measurment for size disritubion(a) and zeta potential(b) of the synthezied nanoparticle

3.3 Heating performance measurement under Near infrared (NIR) laser irradation

Heating characteristics of $Fe@Fe_3O_4$ under NIR irradiation were investigated using DMSA coated nanoparticle containing solution. Before the researches about heating characteristic, light absorptivity of the synthesized nanoparticles was studied for more understand about the effect of concentration on absorption behavior. The absorption spectrum of the nanoparticle were characterized by Lambda 35 UV VIS spectrometer at 500 to 900nm wavelength range. Absorption spectrum of the coated nanoparticles which were illustrated in Figure 3-b does not show significant differences from the previous research works about iron oxide nanopaticles.31,32 Even though the ordinary absorption characteristics about infrared region, the synthesized nanoparticle shows effective heating ability during NIR laser irradiation. The temperature of the sample was raised according to the irradiation time, laser power and solution concentration and the details were described in Figure 5. As a result from Figure 5a and b, the photo derived heat generation of the nanoparticles are linearly proportional to the intensity of the applied laser power at same

concentration. This phenomenon shows that the applied laser is absorbed to a certain degree irrespective of the intensity.

Moreover, the response of the nanoparticles to the concentration change is shown in Figure 5-c and d, and the graph as a whole shows the logarithmic form. This phenomenon is thought to be caused by heat exchange of the solution and surrounding and these convection based heat exchange is linearly proportional to the temperature different between the solution and circumstance air temperature. Therefore, when the temperature change profile is sharply changed at the initial stage of the irradiation and after the certain times when the heat generation and heat loss gets similar value the temperature change of the solution is converged.

However, the tendency of the 10 mg/ml condition is not followed these theoretical basis and it exhibited a little differences compared to 2.5 mg/ml condition. These phenomena were explained by the intrinsic property of the material which the energy conversion ability from light to heat. Therefore, when the concentration is reached certain high value, the particles could not transfer more light to heat anymore. Several previous studies have also supported this

assumption by showing the phenomenon of temperature saturation at high concentrations.33,34

Heat generation=C · ⊿T

Efficiency= (Heat generagtion)/(Irradated energy)

Total heat generation and heat conversion efficiency were calculated by simple mathematical method illustrated above and the calculated data were shown in Table 1. Details about the characters in the equation, C is heat capacitance of solution (4.12 J/K) and T indicates the Celcius degree temperature. From the calculated data, the photothermal conversion efficiency was 33.21 ~ 20.79 % according to the concentration of solution.

Furthermore, we had conducted experiments to figure out the reusability of the synthesized nanoparticles which shown in Figure 5-e. The experiments were carried out by heating the solution with a concentration of 10 mg / ml for 5 minutes in 1 watt laser power. The remaining 4 data except for the first cycle showed almost the same tendency and the average conversion efficiency of the simple

efficiency calculation was 31.13%. The results of this study are as shown in Table 2

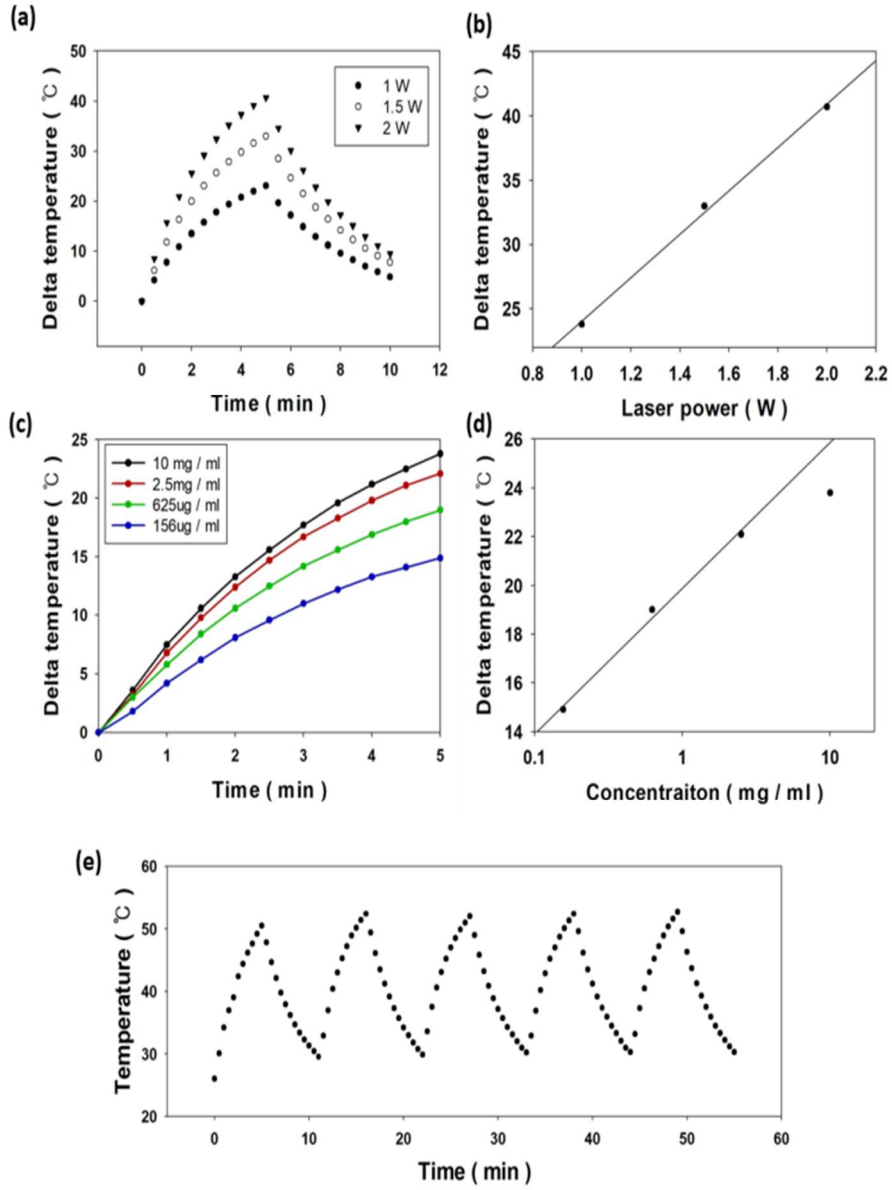

Figure 5 Photothermal characteristics of the synthesized nanoparticles according to the laser power (a), (b), concentration (c), (d) and cycle test (e).

Efficiency according to concentration

C(mg/ml)	10	2.5	0.625	0.156
Efficiency	33.21%	30.84%	26.51%	20.79%

Efficiency according to laser power

Laser P (W)	1	1.5	2
Efficiency	33.21%	30.70%	28.40%

Table 1. Total heat generation and heat conversion efficiency calcuated by simple mathematical method and the results.

	1	2	3	4	5	average (expect 1)
Maximum delta T	24.50	22.90	22.10	22.20	22.40	22.40
Heat Generation (W)	102.56	95.86	92.51	92.93	93.77	93.77
Efficiency	34.19%	31.95%	30.84%	30.98%	31.26%	31.26%

Table 2. Table about the maximum temperature raise, total heat generation and efficiency from photothermal repeating test

3.4 Heating performance measurement under external AC magnetic field

In order to learn about heating characteristics under AC magnetic field, we conducted a magnetic hyperthermia experiment at 150 kHz with various oersted (140-180Oe) and the result is shown in Figue 4. According to the data, magnetic heat generation was amplified by stronger external magnetic field. Theoretically, magnetic hyperthermia is caused by two relaxation mechanisms, Neel and Brownian relaxation. Previous studies have suggested that Neel relaxation is a more important factor when magnetic hyperthermia was studied below 300kHz.35 Also, in general, the total heat generated is linearly proportional to the oersted of the external magnetic field.36 This is due to the fact that the magnetic dipoles of the magnetic nanomaterial are strongly and rapidly aligned by the external electro-magnetic field, and when the AC magnetic field is reversed, there is a correspondingly high degree of alignment to the opposite side. In this process, the spin of the magnetic nanoparticles turns stronger and faster, and as a result, as the intensity of the magnetic field increases, the magnetic hyperthermia effect is promoted.

According to our data illustrated in Figure 6-b shows that the heat generation from electromagnetic field is directly related to the strength of an external electromagnetic field and these results are well matched with the theoretical bases.

Cycle stability under AC magnetic field was also studied and the results are shown in Figure 6-c. The results suggest that Fe@Fe_3O_4 core-shell nanoparticles have sufficient strength to withstand the stress from external magnetic fields. In practice, since most magnetic nanoparticles have a strong resistance to external stimuli, the effect of reducing the efficiency of destruction of materials in general magnetic hyperthermia can be considered insignificant. However, due to the unique magnetic properties of the magnetic nanoparticles, they are magnetized by an external magnetic field. As a result, there are some of retentive magnetism are remained in the particle and this retentive magnetism caused aggregation phenomenon. Moreover, several studies have reported that particle agglomeration has a negative effect on effective hyperthermia. Therefore, high dispersion stability is essential for efficient heat generation.37,38 Briefly, the cycle stability data show the mechanical strength of the Fe@Fe_3O_4 nanoparticles, and it is also evidence that the synthesized nanoparticles do not

aggregate. In addition, the time required for the nanoparticles used in the previous studies to reach the maximum temperature of the application was about ten minutes. However, in the case of our synthesized nanoparticles, the maximum temperature reached within three minutes. This result is reveal that the patient can be treated with a short time of irradiation for magnetic hyperthermia.

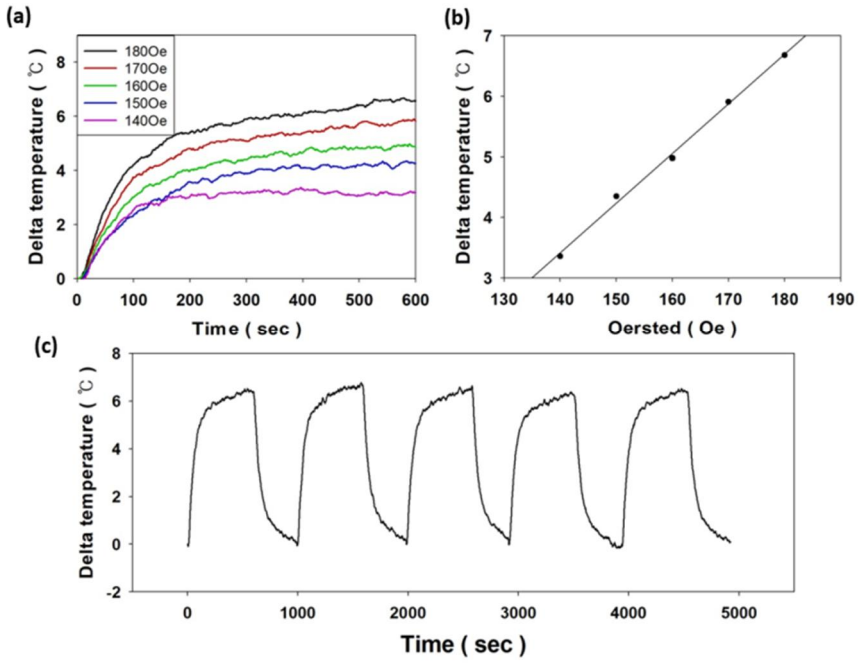

Figure 6 Magnetic hyperthermia characteristics of the synthesized nanoparticles (a), according to the strength of external magnetic field (b) maximum temperature versus various oersted and their fitting curve (linear reference line) (c) cycle test.

Conclusions

In this work, uniform $Fe@Fe_3O_4$ core-shell nanoparticles were synthesized by pyrolysis of iron pentacarbonyl followed by further controlled oxidation. The particles were coated with DMSA for water dispersion. The $Fe@Fe_3O_4$ nanoparticles exhibits effective heating ability and cyclability in near infrared and external AC magnetic field irradiation. Therefore, the synthesized $Fe@Fe_3O_4$ nanoparticles is expected to be good candidate for hyperthermia applications.

References

1 F. Y. Cheng, C. H. Su, Y. S. Yang, C. S. Yeh, C. Y. Tsai, C. L. Wu, M. T. Wu and D. Bin Shieh, Biomaterials, 2005, 26, 729− 738.

2 J. H. Lee, Y. M. Huh, Y. W. Jun, J. W. Seo, J. T. Jang, H. T. Song, S. Kim, E. J. Cho, H. G. Yoon, J. S. Suh and J. Cheon, Nat. Med., 2007, 13, 95− 99.

3 H. Wu, G. Liu, S. Zhang, J. Shi, L. Zhang, Y. Chen, F. Chen and H. Chen, J. Mater. Chem., 2011, 21, 3037− 3045.

4 J. Wang, G. Zhang, Q. Li, H. Jiang, C. Liu, C. Amatore and X. Wang, Sci. Rep., 2013, 3, 1157; DOI:10.1038/srep01157

5 M. Chu, Y. Shao, J. Peng, X. Dai, H. Li, Q. Wu and D. Shi, Biomaterials, 2013, 34, 4078− 4088.

6 P. Guardia, R. Di Corato, L. Lartigue, C. Wilhelm, A. Espinosa, M. Garcia-Hernandez, F. Gazeau, L. Manna and T. Pellegrino, ACS Nano, 2012, 6, 3080− 3091.

7 C. Wilhelm, C. M□nager, M. Curie, F. Gazeau, J. P. Fortin, C. Wilhelm, J. Servais, C. M□nager, J. C. Bacri and F. Gazeau, J. Am. Chem. Soc., 2007, 129, 2628− 2635.

8 J. W. Kim, E. I. Galanzha, E. V. Shashkov, H. M. Moon and V. P. Zharov, Nat. Nanotechnol., 2009, 4, 688− 694.

9 N. H. Cho, T. C. Cheong, J. H. Min, J. H. Wu, S. J. Lee, D. Kim, J. S. Yang, S. Kim, Y. K. Kim and S. Y. Seong, Nat. Nanotechnol., 2011, 6, 675− 682.

10 F. Dilnawaz, A. Singh, C. Mohanty and S. K. Sahoo, Biomaterials, 2010, 31, 3694− 3706.

11 L. Li, F. Tang, H. Liu, T. Liu, N. Hao, D. Chen, X. Teng and J. He, ACS Nano, 2010, 4, 6874-6882.

12 J. Nam, C. Thaxton, and C. Mirkin, Science ., 2003, 301, 1884− 1886.
13 Q. Tian, J. Hu, Y. Zhu, R. Zou, Z. Chen, S. Yang, R. Li, Q. Su, Y. Han and X. Liu, J. Am. Chem. Soc., 2013, 135, 8571− 8577.
14 X. Deng, K. Li, X. Cai, B. Liu, Y. Wei, K. Deng, Z. Xie, Z. Wu, P. Ma, Z. Hou, Z. Cheng and J. Lin, Adv. Mater., 2017, 29, 1701266.
15 X. Huang, S. Tang, B. Liu, B. Ren and N. Zheng, Adv. Mater., 2011, 23, 3420− 3425.
16 Q. Tian, F. Jiang, R. Zou, Q. Liu, Z. Chen, M. Zhu, S. Yang, J. Wang, J. Wang and J. Hu, ACS Nano, 2011, 5, 9761− 9771.
17 S. Sun, H. Zeng, D. B. Robinson, S. Raoux, P. M. Rice, S. X. Wang and G. Li, J. Am. Chem. Soc., 2004, 126, 273− 279.
18 U. I. Tromsdorf, N. C. Bigall, M. G. Kaul, O. T. Bruns, M. S. Nikolic, B. Mollwitz, R. A. Sperling, R. Reimer, H. Hohenberg, W. J. Parak, S. F□rster, U. Beisiegel, G. Adam and H. Weller, Nano Lett., 2007, 7, 2422− 2427.
19 M. M. Cruz, L. P. Ferreira, J. Ramos, S. G. Mendo, A. F. Alves, M. Godinho and M. D. Carvalho, J. Alloys Compd., 2017, 703, 370− 380.
20 E. Mazar□o, J. S□nchez-Marcos, N. Men□ndez, M. Ca□ete, A. Mayoral, S. Rivera-Fern□ndez, J. M. De La Fuente and P. Herrasti, J. Phys. Chem. C, 2015, 119, 6828− 6834.
21 J. H. Lee, J. T. Jang, J. S. Choi, S. H. Moon, S. H. Noh, J. W. Kim, J. G. Kim, I. S. Kim, K. I. Park and J. Cheon, Nat. Nanotechnol., 2011, 6, 418− 422.
22 A. A. El-Gendy, E. M. M. Ibrahim, V. O. Khavrus, Y. Krupskaya, S. Hampel, A. Leonhardt, B. B□chner and R. Klingeler, Carbon, 2009, 47, 2821− 2828.

23 X. Zhao, Z. Zhang, L. Wang, K. Xi, Q. Cao, D. Wang, Y. Yang and Y. Du, Sci. Rep., 2013, 3, 3421; DOI:10.1038/srep03421

24 M. Wu, Y. D. Zhang, S. Hui, T. D. Xiao, S. Ge, W. A. Hines, J. I. Budnick and M. J. Yacaman, J. Appl. Phys., 2002, 92, 6809–6812.

25 S. Peng, C. Wang, J. Xie and S. Sun, J. Am. Chem. Soc., 2006, 128, 10676– 10677.

26 L. M. Lacroix, N. Frey Huls, D. Ho, X. Sun, K. Cheng and S. Sun, Nano Lett., 2011, 11, 1641– 1645.

27 H. Wang, T. B. Shrestha, M. T. Basel, R. K. Dani, G. M. Seo, S. Balivada, M. M. Pyle, H. Prock, O. B. Koper, P. S. Thapa, D. Moore, P. Li, V. Chikan, D. L. Troyer and S. H. Bossmann, Beilstein J. Nanotechnol., 2012, 3, 444– 455.

28 H. Huang, S. Delikanli, H. Zeng, D. M. Ferkey and A. Pralle, Nat. Nanotechnol., 2010, 5, 602– 606.

29 M. Auffan, L. Decome, J. Rose, T. Orsiere, M. De Meo, V. Briois, C. Chaneac, L. Olivi, J. L. Berge-Lefranc, A. Botta, M. R. Wiesner and J. Y. Bottero, Environ. Sci. Technol., 2006, 40, 4367–4373.

30 A. Villanueva, M. C□ete, A. G. Roca, M. Calero, S. Veintemillas-Verdaguer, C. J. Serna, M. Del Puerto Morales and R. Miranda, Nanotechnology, 2009, 20 , 115103

31 A. Espinosa, R. Di Corato, J. Kolosnjaj-Tabi, P. Flaud, T. Pellegrino and C. Wilhelm, ACS Nano, 2016, 10, 2436– 2446.

32 L. Sen Lin, Z. X. Cong, J. B. Cao, K. M. Ke, Q. L. Peng, J. Gao, H. H. Yang, G. Liu and X. Chen, ACS Nano, 2014, 8, 3876–3883.

33 J. Chen, X. Wang and T. Chen, Nanoscale Res. Lett., 2014, 9, 86.

34 Z. Zha, X. Yue, Q. Ren, and Z. Dai, Adv. Mater., 2013, 25, 777-782

35 X. Zhang, S. Chen, H.-M. Wang, S.-L. Hsieh, C.-H. Wu, H.-H. Chou and S. Hsieh, Biomed. Eng. Appl. Basis Commun., 2010, 22, 393− 399.

36 B. Mehdaoui, A. Meffre, J. Carrey, S. Lachaize, L. M. Lacroix, M. Gougeon, B. Chaudret and M. Respaud, Adv. Funct. Mater., 2011, 21, 4573− 4581.

37 X. Wang, H. Gu and Z. Yang, J. Magn. Magn. Mater., 2005, 293, 334− 340.

38 A. E. Deatsch and B. A. Evans, J. Magn. Magn. Mater., 2014, 354, 163− 172.

국 문 초 록

근적외선 (NIR) 레이저 조사 또는 외부 AC 자기장 적용 하에서 $Fe@Fe_3O_4$ 코어 쉘 나노 입자의 가열 특성

자성 나노 입자는 고열 치료에 사용할 수 있는 고유의 자기 특성으로 인해 많은 관심을 받았습니다. 본 연구에서는 근적외선 레이저 조사 또는 외부 교류 자기장인가시 $Fe@Fe_3O_4$ 코어-쉘 나노 입자의 가열 특성을 연구하였습니다. $Fe@Fe_3O_4$ 코어 쉘 나노 입자는 철 펜타카보닐의 열 분해를 통해 합성된 철 나노 입자의 부분적 산화에 의해 합성되었습니다. 투과 전자 현미경 분석을 통해 9.6 ± 1.1 nm 의 철 코어를 갖는 총 14.9 ± 1.2 nm 의 크기의 나노입자를 관찰 했으며, 자력계 측정을 통해 코어 – 쉘 나노 입자의 자기 포화 값이 83.3 emu / g 임을 확인하였습니다. 추가 실험을 위해, 합성된 나노입자 표면에 dimercaptosuccinic acid 를 코팅하여 $Fe@Fe_3O_4$ 입자의 수분산성을 증대 시켰고, 수분산 용액을 이용하여 근적외선 레이저와 AC 자기장 하에서의 발열 특성을 연구했습니다. 근적외선 레이저 조사 또는 AC 자기장인가 하에서 합성된

입자는 효과적인 가열 능력을 보여주었습니다. 광열효과에 대한 연구는 808nm 근적외선 레이저를 이용하여 수행하였고, 1watt / cm2 전력 밀도에서 나노 입자를 포함하는 용액의 온도는 14.9 ~ 23.8 ℃ 증가하였고 용액 농도와 레이저 출력이 증가함에 따라 온도 상승은 더 커졌습니다. 또한 외부 자기장에 의한 발열효과는 주파수 (150kHz)와 다양한 에르스테드 (140 ~ 180Oe) 조건에서 연구되었으며, 인가 된 교류 자기장 하에서 용액의 온도는 조건에 따라 1.5 ~ 6.6 ℃ 상승 하였습니다. 이를 통해 합성된 나노입자가 광열과 자기장 발열효과를 모두 보여주어 잠재적인 온열치료 입자로 사용될 수 있음을 확인하였습니다.

주요어: 자성 입자, 코어-쉘 나노입자, 표면 처리, 자기장 온열치료, NIR 레이저 온열 치료

학번: 2017-25795